Journal of Nuclear Materials 405 (2010) 186–198

Contents lists available at ScienceDirect

Journal of Nuclear Materials

journal homepage: www.elsevier.com/locate/jnucmat

Thermodynamic assessment of the LiF–NaF–ThF_4–UF_4 system

O. Beneš *, M. Beilmann, R.J.M. Konings

European Commission, Joint Research Centre, Institute for Transuranium Elements, P.O. Box 2340, 76125 Karlsruhe, Germany

ARTICLE INFO

Article history:
Received 12 July 2010
Accepted 14 August 2010

ABSTRACT

A thermodynamic assessment of the LiF–NaF–ThF_4–UF_4 system is presented in this study. The binary phase diagrams are optimized based on the known experimental data and the excess Gibbs energies of liquid and solid solutions are described using a modified quasi chemical model and polynomial formalism respectively. The higher order systems are extrapolated according to asymmetric Toop mathematical formalism. Based on the developed thermodynamic database the fuel composition of the molten salt fast reactor is optimized. In total three different fuel compositions are identified. Properties of these fuel compositions such as melting point, vapour pressure and the boiling temperature are derived from the obtained thermodynamic assessment and are presented in this study.

1. Introduction

The Molten Salt Reactor (MSR) is one of the six reactor concepts of the Generation IV (GenIV) initiative. In this concept, the fissile material (^{233}U, ^{235}U and ^{239}Pu) is dissolved in the molten fluoride matrix circulating in the primary circuit from the reactor core to the heat exchanger and back. Compared to solid fuel reactors, the advantage of the MSR is the possibility of fuel purification during the operation. Since the salt is in the liquid form it can be extracted, either online or in batches, and cleaned from the fission products in an on-site chemical re-processing plant. This process increases the effectiveness of the reactor because most of the fission products cause parasitic neutron capture and their accumulation slows down the chain reaction. Currently there are two main approaches of the MSR. The first are moderated and non-moderated breeder reactors based on the $^{232}Th/^{233}U$ cycle, for which respectively $^{7}LiF–BeF_2$ and ^{7}LiF are considered as an ideal matrix due to the very low parasitic neutron capture cross section of given cations. When designed as an actinide burner the fuel will be most likely PuF_3 with possibly small addition of minor actinide tri- or tetra-fluorides (AmF_3, NpF_4, etc.). To achieve a favourable melting temperature of the fuel, the matrix based on the $^{7}LiF–NaF–BeF_2$ system is the prime candidate.

In this study, we develop a thermodynamic database of the LiF–NaF–UF_4–ThF_4 system and based on the obtained results we optimize the fuel composition of the molten salt fast reactor (MSFR) concept [1]. In order to create such a database we first assess the binary sub-systems based on the available experimental data and afterwards the higher order systems are extrapolated according to the Toop mathematical formalism. This approach was shown as a very strong tool of predicting the fuel behaviour as demonstrated in previous studies [2–4]. Furthermore once the thermodynamic database is developed properties such as melting temperature, vapour pressure or solubility of actinide fluorides in the fuel matrix can be calculated. All of these properties are very important quantities for the nuclear reactor design; hence the knowledge of the thermodynamic database is of importance. The initial matrix of the molten salt fast reactor is based only on the pure ^{7}LiF compound, however, as shown in this study the melting temperature of the fuel based only on a single component solvent is rather high, around 840 K. This is also the main reason that the designed inlet temperature of this reactor concept is set relatively high, far above 900 K. One of the possible solutions to decrease the melting temperature of the fuel is to add another matrix component. Therefore, one of the objectives of this work was to investigate the effect of the NaF addition as another possible component in the fuel solvent. It has been found that such addition has significant influence on the melting behaviour decreasing the melting point of the fuel by more than 50 K.

2. Thermodynamic modelling

All thermodynamic calculations performed in this study were done using the FactSage software [5], based on the Gibbs energy minimization. The unknown thermodynamic quantities that are necessary for the phase diagram calculations, in our case the excess Gibbs energies of the liquid and solid solutions plus the thermodynamic data of the intermediate solid compounds, were obtained during the phase diagram optimization in such way that the best possible agreement between the experimentally determined equilibrium data and the calculation has been achieved.

2.1. Pure compounds

The Gibbs energy function above the room temperature for pure compounds is defined as:

* Corresponding author. Tel.: +49 7247 951 385; fax: +49 7247 951 99385.
E-mail address: ondrej.benes@ec.europa.eu (O. Beneš).

0022-3115/$ - see front matter © 2010 Elsevier B.V. All rights reserved.
doi:10.1016/j.jnucmat.2010.08.017

$$G(T) = \Delta_f H^0(298) - S^0(298)T + \int_{298}^{T} C_p(T)dT - T\int_{298}^{T}\left(\frac{C_p(T)}{T}\right)dT \quad (1)$$

where $\Delta_f H^0(298)$ and $S^0(298)$ are the standard enthalpy of formation, respectively standard absolute entropy, both referring to a temperature of 298.15 K. The $C_p(T)$ term is the temperature function of heat capacity at constant pressure.

The thermodynamic data of pure LiF and NaF compounds were taken from [6], while the data of the ThF_4 and UF_4 end-members were taken from [7]. To our best knowledge no data are known for the intermediate compounds of the LiF–NaF–ThF_4–UF_4 system so these had to be assessed. The heat capacity of all intermediate phases was estimated based on the Neumann–Kopp rule whereas the standard enthalpy of formation and the absolute entropy at 298.15 K have been optimized during the phase diagram assessment.

The thermodynamic data of all stoichiometric phases used in this study are summarized in Table 1.

2.2. Solid solutions

For the description of the excess Gibbs parameters of solid solutions a polynomial formalism has been used. The total Gibbs energy of such solution is given by the following equation:

$$G(T) = X_1 \cdot G^{\circ}_{m,1}(T) + X_2 \cdot G^{\circ}_{m,2}(T) + X_1 RTlnX_1 + X_2 RTlnX_2 + G^{xs}_m \quad (2)$$

where G°_m is the molar standard Gibbs energy of pure end-members,

$$G^{xs}_m = \sum_{i,j} X^i_1 \cdot X^j_2 \cdot L_{i,j} \quad (3)$$

and X_1 and X_2 are the mole fractions of the mixed end-members. The $L_{i,j}$ term from Eq. 3 is the general equation:

$$L_{i,j} = A + BT + CTlnT + DT^2 \ldots \quad (4)$$

with parameters to be optimized during the thermodynamic assessment.

The values of the excess Gibbs parameters of various solid solutions considered in this study are summarized in Table 2. The data for the (Li, Na)F solid solution were adopted from our previous study [8]. In case of the $(Li, Na)_7Th_6F_{31}$ solid solution the standard Gibbs energy function of the hypothetical $Li_7Th_6F_{31}$ end-member had to be assessed as well and the obtained value is reported in the same table.

2.3. Liquid solution

The modified quasichemical model presented by Pelton et al. [9] and Chartrand et al. [10] has been used to optimize the excess

Table 2
The excess Gibbs energy functions of solid solutions considered in this study.

Solid solution	ΔG^{xs} (J mol^{-1})
(Li, Na)F	$\Delta G^{xs} = X_{LiF} \cdot X_{NaF} \cdot 22,250 + X^3_{LiF} \cdot X_{NaF} \cdot 17,250$
$(Na_x, Th_{1-x})F_{4-3x}$	$\Delta G^{xs} = X_{NaF} \cdot X_{ThF_4} \cdot (-15,500) + X^3_{NaF} \cdot X_{ThF_4} \cdot 40,000$
(Th, U)F_4	$\Delta G^{xs} = X_{ThF_4} \cdot X_{UF_4} \cdot 1600$
$(Li, Na)_7Th_6F_{31}$	$\Delta G^{xs} = X_{Li_7Th_6F_{31}} \cdot X_{Na_7Th_6F_{31}} \cdot (-75,000) + X_{Li_7Th_6F_{31}} \cdot X^2_{Na_7Th_6F_{31}} \cdot (-150,000)$ $G^{\circ}_{Li_7Th_6F_{31}\_ss} = G^{\circ}_{Li_7Th_6F_{31}} + 30,000$
$(Li, Na)_7U_6F_{31}$	$\Delta G^{xs} = X_{Li_7U_6F_{31}} \cdot X_{Na_7U_6F_{31}} \cdot (7000) + X_{Li_7U_6F_{31}} \cdot X^2_{Na_7U_6F_{31}} \cdot (12,500)$
Li(Th, U)$_4F_{17}$	$\Delta G^{xs} = X_{LiTh_4F_{17}} \cdot X_{LiU_4F_{17}} \cdot (-45,000)$
Li(Th, U)$_2F_9$	$\Delta G^{xs} = X_{LiTh_2F_9} \cdot X_{LiU_2F_9} \cdot (-15,000)$
Li_7(Th, U)$_6F_{31}$	$\Delta G^{xs} = X_{Li_7Th_6F_{31}} \cdot X_{Li_7U_6F_{31}} \cdot (-75,000)$
Li_3(Th, U)F_7	$\Delta G^{xs} = X_{Li_3ThF_7} \cdot X_{Li_3UF_7} \cdot (-8000)$
Na_7(Th, U)$_2F_{15}$	$\Delta G^{xs} = X_{Na_7Th_2F_{15}} \cdot X_{Na_7U_2F_{15}} \cdot (-135,000)$
Na_2(Th, U)F_6	$\Delta G^{xs} = X_{Na_2ThF_6} \cdot X_{Na_2UF_6} \cdot (13,500) + X^2_{Na_2ThF_6} \cdot X_{Na_2UF_6} \cdot (12,500) + X_{Na_2ThF_6} \cdot X^2_{Na_2UF_6} \cdot (-15,000)$
Na_7(Th, U)$_6F_{31}$	$\Delta G^{xs} = X_{Na_7Th_6F_{31}} \cdot X_{Na_7U_6F_{31}} \cdot (-90,000)$
Na(Th, U)$_2F_9$	$\Delta G^{xs} = X_{NaTh_2F_9} \cdot X_{NaU_2F_9} \cdot (-6000)$
$Na_3Th_2F_{11}$–$Na_5U_3F_{17}$	$\Delta G^{xs} = X_{Na_3Th_2F_{11}} \cdot X_{Na_5U_3F_{17}} \cdot (-30,000)$

Table 1
The $\Delta_f H^0(298.15)$ (kJ mol^{-1}), $S^0(298.15)$ (J K^{-1} mol^{-1}) and C_p (J K^{-1} mol^{-1}) data of pure compounds used in this study.

Compound	$\Delta_f H^0(298.15)$	$S^0(298.15)$	$C_p = a + bT + cT^2 + dT^{-2}$			
			a	$b\,T$	$c\,T^2$	$d\,T^{-2}$
LiF (s)	−616.931	35.66	43.309	1.6312×10^{-2}	5.0470×10^{-7}	−569124
LiF (l)	−598.654	42.962	64.183	–	–	–
NaF (s)	−576.650	51.21	47.630	1.4790×10^{-2}	–	−464300
NaF (l)	−557.730	52.755	72.989	–	–	–
ThF_4 (s)	−2097.900	142.05	122.173	8.3700×10^{-3}	–	−1255000
ThF_4 (l)	−2064.491	156.629	133.9	–	–	–
UF_4 (s)	−1914.200	151.70	114.519	2.0555×10^{-2}	–	−413159
UF_4 (l)	−1914.658	115.400	174.74	–	–	–
Li_3ThF_7 (s)	−3963.393	249.0	252.100	5.7307×10^{-2}	1.5141×10^{-6}	−2962371
$Li_7Th_6F_{31}$ (s)	−16974.917	1101.92	1036.201	1.6441×10^{-1}	3.5329×10^{-6}	−11513865
$LiTh_2F_9$ (s)	−4829.731	320.76	287.655	3.3052×10^{-2}	5.0470×10^{-7}	−3079124
$LiTh_4F_{17}$ (s)	−9031.431	603.86	532.001	4.9792×10^{-2}	5.0470×10^{-7}	−5589124
Li_4UF_8 (s)	−4347.620	357.55	287.755	8.5804×10^{-2}	2.0188×10^{-6}	−2689653
$Li_7U_6F_{31}$ (s)	−15826.900	1230.82	990.279	2.3751×10^{-1}	3.5329×10^{-6}	−6462819
LiU_4F_{17} (s)	−8293.761	644.70	501.387	9.8532×10^{-2}	5.0470×10^{-7}	−2221760
Na_4ThF_8 (s)	−4355.195	450.4	312.693	6.7530×10^{-2}	–	−3112200
$Na_7Th_2F_{15}$ (s)	−8285.600	677.6	577.756	1.2027×10^{-1}	–	−5760100
Na_2ThF_6 (s)	−3282.870	255.9	217.433	3.7950×10^{-2}	–	−2183600
$Na_3Th_2F_{11}$ (s)	−5910.275	526.4	387.236	6.1110×10^{-2}	–	−3902900
$Na_7Th_6F_{31}$ (s)	−16653.219	1364.0	1066.448	1.5375×10^{-1}	–	−10780100
$NaThF_5$ (s)	−2693.871	199.2	169.803	2.3160×10^{-2}	–	−1719300
$NaTh_2F_9$ (s)	−4791.776	348.3	291.976	3.1530×10^{-2}	–	−2974300
Na_3UF_7-α (s)	−3633.100	366.5	257.409	6.4925×10^{-2}	–	−1806059
Na_3UF_7-β (s)	−3632.600	367.1	257.409	6.4925×10^{-2}	–	−1806059
Na_2UF_6 (s)	−3089.500	272.3	209.779	5.0135×10^{-2}	–	−1341759
$Na_5U_3F_{17}$ (s)	−8623.600	828.5	581.708	1.3561×10^{-1}	–	−3560977
$Na_7U_6F_{31}$ (s)	−15608.800	1363.984	1020.526	2.2686×10^{-1}	–	−5729054
NaU_2F_9 (s)	−4430.200	354.6	276.669	5.5900×10^{-2}	–	−1290618

Gibbs functions of the liquid solution. Using this model it is possible to freely permit the choice of the composition of maximum short range ordering in a binary system which is done by the definition of cation–cation coordination numbers $Z^A_{AB/FF}$, resp. $Z^B_{AB/FF}$. This selection is of importance in terms of thermodynamic modelling as the excess Gibbs function of the solution tends to have its minimum here. The values of the cation-cation coordination numbers $Z^A_{AB/FF}$ and $Z^B_{AB/FF}$ that have been used in this study are reported in Table 3. Since these coordination numbers correspond exactly to one point where the maximum short range ordering is expected they are composition independent.

In order to keep the electro-neutrality in the system, the definition of the anion–anion coordination numbers is required. These are calculated according to the following equation after the selection of the cation–cation coordination numbers.

$$\frac{q_A}{Z^A_{AB/FF}} + \frac{q_B}{Z^B_{AB/FF}} = \frac{q_F}{Z^F_{AB/FF}} + \frac{q_F}{Z^F_{AB/FF}} \tag{5}$$

The q_A, q_B and q_F terms in the above given formula are the absolute charges of various ions.

The parameters of the modified quasichemical model are the Gibbs energy changes $\Delta g_{AB/F}$ for the second nearest neighbor (SNN) pair–exchange reaction:

$$(A-F-A)+(B-F-B)=2(A-F-B) \quad \Delta g_{AB/F} \tag{6}$$

where A and B represent the cations and F the F^- anion as the only anion considered in this study. The $\Delta g_{AB/F}$ parameter for reaction (6) can be expanded as a polynomial such as:

$$\Delta g_{AB/F} = \Delta g^0_{AB/F} + \sum_{(i+j)\geqslant q1} g^{ij}_{AB/F}\chi^i_{AB/F}\chi^j_{BA/F} \tag{7}$$

where $\Delta g^0_{AB/F}$ and $g^{ij}_{AB/F}$ are composition independent coefficients (although possibly temperature dependent) obtained from the optimization of the experimental data for binary $AF-BF$ solutions. The $\chi_{AB/F}$ term is a composition variable and is defined as:

$$\chi_{AB/F} = \left(\frac{X_{AA}}{X_{AA}+X_{AB}+X_{BB}}\right) \tag{8}$$

Table 3
Cation–cation coordination numbers of the liquid.

A	B	Z^A_{AB}	Z^B_{AB}
Li^+	Li^+	6	6
Na^+	Na^+	6	6
Th^{4+}	Th^{4+}	6	6
U^{4+}	U^{4+}	6	6
Li^+	Na^+	6	6
Li^+	Th^{4+}	2	6
Li^+	U^{4+}	2	6
Na^+	Th^{4+}	2	6
Na^+	U^{4+}	3	6
Th^{4+}	U^{4+}	6	6

The excess Gibbs parameters for the binary sub-systems of the LiF–NaF–ThF_4–UF_4 system are listed below keeping the same notation as proposed by Chartrand and Pelton [11]. All presented values were optimized in this work except the data for the LiF–NaF system which were taken from our previous study [12]. For the ThF_4–UF_4 system no excess data for the liquid solution are presented as it was treated ideally.

$$\Delta g_{LiNa/FF} = -2307.47 + 0.4281T \quad \text{J mol}^{-1} \tag{9}$$

$$\Delta g_{LiTh/FF} = -15,983 + 2.092T - 2929\chi_{LiTh} + (-28,024 + 20.92T)\chi_{ThLi} \quad \text{J mol}^{-1} \tag{10}$$

$$\Delta g_{LiU/FF} = -16,108 + (-711.3 - 1.255T)\chi_{LiU} + (-1172 - 8.368T)\chi_{ULi} \quad \text{J mol}^{-1} \tag{11}$$

$$\Delta g_{NaTh/FF} = -28,033 + (10,042 - 12.552T)\chi_{NaTh} + (-23,012 + 8.368T)\chi_{ThNa} \quad \text{J mol}^{-1} \tag{12}$$

$$\Delta g_{NaU/FF} = -25,104 + 4.184T + (-7615 - 4.184T)\chi_{NaU} + (-14,393 + 6.276T)\chi_{UNa} \quad \text{J mol}^{-1} \tag{13}$$

2.4. Gas phase

One of the outcome of this study was the determination of the vapour pressure of the molten salt fuel, hence the solid–gas and liquid–gas equilibria had to be considered in this study as well. Since relatively small vapour pressures ($\ll$1 bar) were subject of our calculations the gas phase was treated ideally. The thermodynamic data for the gas species used in this study are summarized in Table 4.

2.5. Higher order systems

Once the binary phase diagrams are assessed the higher order systems can be extrapolated according to several mathematical formalisms. In this study, the excess Gibbs energies of the higher order liquid solutions of the LiF–NaF–ThF_4–UF_4 system were extrapolated based on the asymmetric Toop formalism keeping two groups of symmetry. The first one composed of alkali fluorides (LiF, NaF) which typically form ionic species in the liquid while the other one consists of ThF_4 and UF_4 compounds that are known to form rather molecular species in the liquid state.

There are four ternary systems presented in this study. The excess Gibbs energies of the ternary liquid solution of two of them (LiF–NaF–ThF_4 and LiF–UF_4–ThF_4) have been calculated purely based on the corresponding binary sub-systems, in case of the LiF–NaF–UF_4 and NaF–UF_4–ThF_4 systems some additional ternary

Table 4
The $\Delta_f H^0(298.15)$ (kJ mol^{-1}),$S^0(298.15)$ (J K^{-1} mol^{-1}) and $C_p = a + bT + cT^2 + dT^{-2} + eT^3$ (J K^{-1} mol^{-1}) data of gaseous species considered in this study.

Compound	$\Delta_f H^0_{(298.15)}$	$S^0_{(298.15)}$	a	$b\,T$	$c\,T^2$	$d\,T^{-2}$	$e\,T^3$	Reference
LiF(g)	−340.946	200.19	35.40	0.001871	-1.6543×10^{-7}			[6]
Li_2F_2(g)	−935.323	261.80	83.09	1×10^{-5}		−2170730		[6]
Li_3F_3(g)	−1524.598	316.70	132.92	3×10^{-5}		−3747001		[6]
NaF(g)	−295.158	217.50	36.98	0.000789	1.2644×10^{-7}			[6]
Na_2F_2(g)	−834.063	297.79	83.14	2.1051×10^{-6}		−820673		[6]
ThF_4(g)[a]	−1748.200	351.56	122.41	−0.01406	7.3654×10^{-6}		-1.9395×10^{-9}	[13]
UF_2(g)	−535.037	315.70	50.17	0.02168		−35735.3	-5.6798×10^{-5}	[13]
UF_3(g)	−1060.959	347.79	81.33	-4.3×10^{-6}	2.4270×10^{-6}	−476300		[13]
UF_4(g)	−1605.200	360.7	103.83	0.009549	-1.4510×10^{-6}	−1021320		[13]

[a] Extra terms were used for the heat capacity: 2.0108E−13 · T^4 and −7544.6 · T^{-1}.

parameters had to be introduced in order to better reproduce the liquidus temperatures measured by Thoma et al. [14] and the ternary invariant equilibria experimentally determined by Thoma et al. [15] respectively. The obtained parameters are given below:

$$g^{001}_{\mathrm{LiNa(U)}/FF} = 12,550\ \mathrm{J\ mol^{-1}} \quad (14)$$

$$g^{001}_{\mathrm{ULi(Na)}/FF} = 4200\ \mathrm{J\ mol^{-1}} \quad (15)$$

$$g^{001}_{\mathrm{UNa(Li)}/FF} = 2100\ \mathrm{J\ mol^{-1}} \quad (16)$$

$$g^{001}_{\mathrm{ThU(Na)}/FF} = 3770\ \mathrm{J\ mol^{-1}} \quad (17)$$

3. Binary systems

As mentioned in the previous section, a good thermodynamic description of binary systems is the basis for the prediction of any multi-component system. Therefore, in order to create the LiF–NaF–ThF_4–UF_4 thermodynamic database all six binary sub-systems must be assessed. First of them, the LiF–NaF system, is a single eutectic system with limited solubility in the solid state at the NaF rich side. This phase diagram has been presented in our previous studies [12,8] which we refer to for details. The five remaining systems (LiF–ThF_4, LiF–UF_4, NaF–ThF_4, NaF–UF_4 and ThF_4–UF_4) have been optimized in this study and are discussed in the following sub-sections.

3.1. The LiF–ThF_4 system

The optimization of the LiF–ThF_4 system was based on the thermal analysis data reported by Thoma et al. [16]. The calculated LiF–ThF_4 phase diagram obtained in this study is shown in Fig. 1. It consists of five invariant equilibria; Two eutectics found at $T = 841$ K and $X(ThF_4) = 0.234$ and $T = 840$ K and $X(ThF_4) = 0.276$ and three peritectics found at $T = 870$ K and $X(ThF_4) = 0.306$ where $Li_7Th_6F_{31}$ decomposes, $T = 1035$ K and $X(ThF_4) = 0.425$ assigned to the $LiTh_2F_9$ decomposition and $T = 1170$ K and $X(ThF_4) = 0.592$ where the $LiTh_4F_{17}$ phase decomposes. The Li_3ThF_7 intermediate compound that appears in this binary system melts congruently at $T = 842$ K. All equilibria are in perfect agreement with the data of Thoma et al. as obvious from Fig. 1.

In the study by Thoma et al. [16] the $Li_7Th_6F_{31}$ phase is reported whereas the later study [17] by the same authors shows rather equimolar $LiThF_5$ phase instead of the 7:6 phase. However, no details or comments are given in that reference therefore the option with the 7:6 phase is kept in our assessment as X-ray diffraction patterns for this phase have been shown in the earlier work by Thoma et al. [16] and by Harris et al. [18]. This assumption is in contrast to the thermodynamic assessment of the LiF–ThF_4 system done recently by van der Meer et al. [19] who considered rather the 1:1 phase. Nevertheless, it has been observed in this study that the selection of the 'correct' intermediate phase hardly affects the liquidus line in the equilibrium phase diagram.

3.2. The LiF–UF_4 system

The LiF–UF_4 phase diagram has been optimized based on the experimental data taken from Barton et al. [20]. They used thermal analysis, quenching technique and visual observation methods closely coupled with X-ray diffraction analysis to identify the equilibrium points. The assessed LiF–UF_4 phase diagram is shown in Fig. 2. It consists of three intermediate phases, all of them melting peritectically. The $Li_7U_6F_{31}$ and LiU_4F_{17} compounds are stable at room temperature whereas the Li_4UF_8 phase has limited range of stability with lower decomposition limit at $T = 743$ K. The peritectic invariant equilibria calculated in our study were found at $T = 774$ K and $X(UF_4) = 0.253$ corresponding with the Li_4UF_8 decomposition, $T = 883$ K and $X(UF_4) = 0.403$ corresponding with the $Li_7U_6F_{31}$ decomposition and $T = 1048$ K and $X(UF_4) = 0.576$ assigned with the LiU_4F_{17} decomposition. The lowest melting point of the LiF–UF_4 system was found at the binary eutectic at $T = 761$ K and $X(UF_4) = 0.266$. As shown in Fig. 2, all calculated invariant equilibria agree very well to the experimental data [20].

3.3. The NaF–ThF_4 system

The thermodynamic assessment of the NaF–ThF_4 system has been based on the equilibrium data published by Thoma et al. [16] and Thoma [17]. The system is characterized by three peritectic and three eutectic invariant equilibria. A comparison between the calculated values and the experimental data [16] of all invariant equilibria found in this binary system is given in Table 5 indicating fairly good overall agreement. The NaF–ThF_4 system consists of seven intermediate compounds. Na_4ThF_8 has a very small stability range having the low temperature decomposition limit at $T = 883$ K and melting peritectically at $T = 920$ K. The $Na_7Th_2F_{15}$ compound has a lower stability limit at $T = 829$ K and decomposes to Na_4ThF_8 and Na_2ThF_6 at 884 K. The Na_2ThF_6 phase is stable from the room temperature and melts congruently at $T = 978$ K.

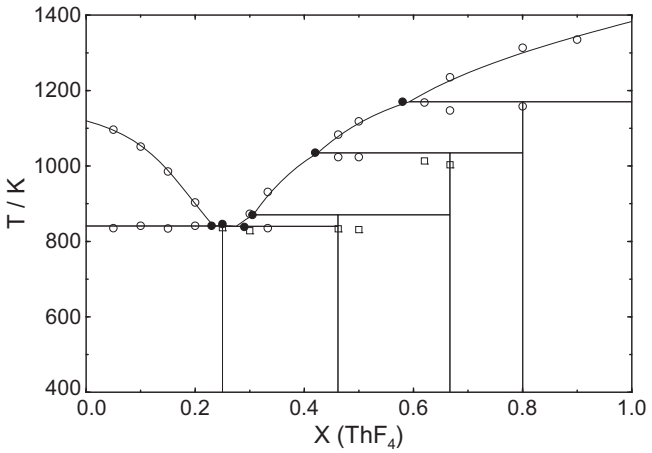

Fig. 1. The optimized LiF–ThF_4 phase diagram; ○ thermal analysis data obtained by Thoma et al. [16], □ supercooled data, • invariant equilibria as reported in [16].

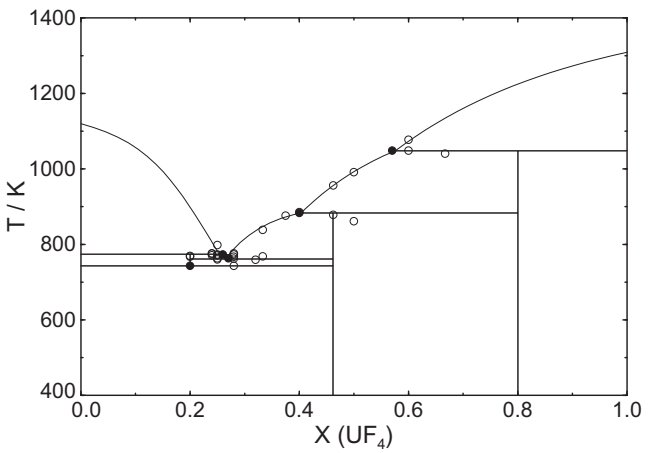

Fig. 2. The optimized LiF–UF_4 phase diagram; ○ data obtained by Barton et al. [20] by quenching of LiF–UF_4 mixtures, •invariant equilibria as reported in [20].

Table 5
Invariant equilibria in the NaF–ThF_4 system.

X_{calc} (ThF_4)[a]	T_{calc}[a] (K)	X_{exp} (ThF_4)[b]	T_{exp}[b] (K)	Equilibrium	Phases in equilibrium[c]
0.200	883	0.200	877[d]	Lower decomposition limit	Na_4ThF_8 + NaF + $Na_7Th_2F_{15}$
0.216	920	0.215	918	Peritectic	L + Na_4ThF_8 + NaF
0.231	901	0.225	891	Eutectic	L + Na_4ThF_8 + Na_2ThF_6
0.222	830	0.222	831	Lower decomposition limit	NaF + $Na_7Th_2F_{15}$ + Na_2ThF_6
0.222	884	0.222	883[d]	Upper decomposition limit	Na_4ThF_8 + $Na_7Th_2F_{15}$ + Na_2ThF_6
0.333	978	0.333	978	Congruent melting	L + Na_2ThF_6
0.362	977	0.370	963	Eutectic	L + $Na_3Th_2F_{11}$ + Na_2ThF_6
0.400	955	0.400	956	Lower decomposition limit	$Na_3Th_2F_{11}$ + $Na_7Th_6F_{31}$ + Na_2ThF_6
0.400	985	0.400	985	Congruent melting	L + $Na_3Th_2F_{11}$
0.401	985	0.410	978	Eutectic	L + $Na_3Th_2F_{11}$ + $Na_7Th_6F_{31}$
0.449	1001	0.455	1003	Peritectic	L + $Na_7Th_6F_{31}$ + $NaTh_2F_9$
0.462	883	–	–	Lower decomposition limit	Na_2ThF_6 + $Na_7Th_6F_{31}$ + $NaThF_5$
0.500	893	–	–	Upper decomposition limit	$NaTh_2F_9$ + $Na_7Th_6F_{31}$ + $NaThF_5$
0.559	1087	0.580	1104	Peritectic	L + $(Na_{1-x}Th_x)F_{3x+1}$ + $NaTh_2F_9$

[a] Obtained in this study.
[b] Experimentally determined by Thoma et al. [16].
[c] Symbol 'L' refers to liquid.
[d] Experimentally determined by Thoma [17].

$Na_3Th_2F_{11}$ is another congruently melting phase with melting point at T = 985 K and lower decomposition limit of 955 K. The $Na_7Th_6F_{31}$ compound is stable from 883 K to the peritectic melting at T = 1001 K whereas $NaThF_5$ is stable from room temperature and decomposes below solidus at 893 K to $NaTh_2F_9$ and $Na_7Th_6F_{31}$. $NaTh_2F_9$ is stable from room temperature and decomposes peritectically at 1086 K. Furthermore a limited solid solution appears at the ThF_4 rich side with maximum solubility limit of 11 mol% of LiF in the solid ThF_4 matrix at the peritectic temperature, T = 1086 K. This value is in agreement with the NaF–ThF_4 phase diagram published by Thoma et al. [16]. The optimized phase diagram obtained in this study is shown in Fig. 3.

3.4. The NaF–UF_4 system

The NaF–UF_4 system has been investigated by the same authors [20] as the LiF–UF_4 system discussed above applying the same experimental techniques. Based on these data the binary phase diagram has been assessed and is shown in Fig. 4. It consists of ten invariant equilibria, three eutectics, two peritectics where Na_2UF_6 and $Na_5U_3F_{17}$ decompose, two congruent melting points of the Na_3UF_7 and $Na_7U_6F_{31}$ intermediate compounds and three decomposition limits of Na_3UF_7, $Na_5U_3F_{17}$ and NaU_2F_9. The lowest

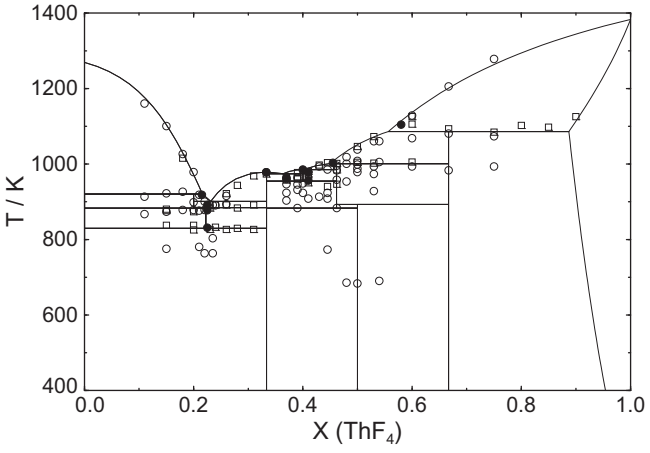

Fig. 3. The optimized NaF–ThF_4 phase diagram; ○ thermal analysis data from [16], □ data obtained by quenching of NaF–ThF_4 mixtures taken from [16], • invariant equilibria as reported in [16].

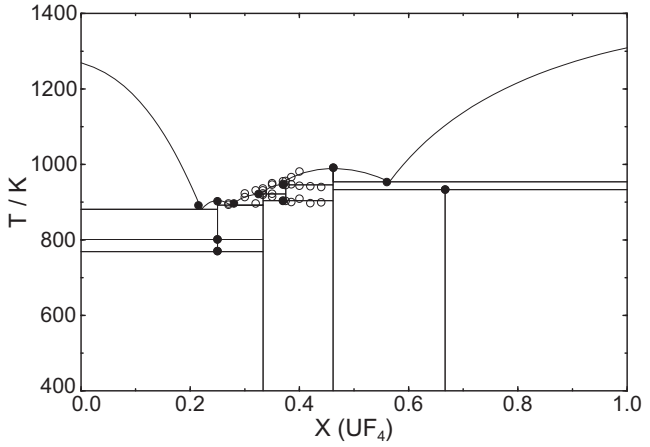

Fig. 4. The optimized NaF–UF_4 phase diagram; ○ data obtained by quenching of NaF–UF_4 mixtures taken from [20], • invariant equilibria as reported in [20].

eutectic was found at T = 881 K and $X(UF_4)$ = 0.220 which is slightly lower than the proposed eutectic given by [20]. All invariant equilibria are summarized in Table 6 where a comparison to the experimental data is made showing an excellent overall agreement.

Out of five intermediate compounds found in the NaF–UF_4 system Na_2UF_6, $Na_7U_6F_{31}$ and NaU_2F_9 are stable from the room temperature, the last one decomposing below solidus at T = 933 K whereas the Na_3UF_7 and $Na_5U_3F_{17}$ compounds have lower decomposition limits at T = 769 K and T = 904 K respectively. It was observed by Barton et al. [20] that the Na_3UF_7 compound undergoes a transition in the solid state at T = 801 K.

3.5. The ThF_4–UF_4 system

As reported by Weaver et al. [21], the ThF_4–UF_4 system is characterized by a continuous solid solution with no minimum at solidus and liquidus equilibria. The same authors performed a thermal analysis of this system publishing only limited amount of experimental data. Based on these data the ThF_4–UF_4 phase diagram has been assessed treating the liquid solution ideal while small positive excess Gibbs parameters had to be introduced for the description of the (Th, U)F_4 solid solution in order to best fit the experimental data. The optimized phase diagram obtained in this study is shown in Fig. 5 having a very similar shape to the

Table 6
Invariant equilibria in the NaF–UF_4 system.

X_{calc} (UF_4)[a]	T_{calc}[a] (K)	X_{exp} (UF_4)[b]	T_{exp}[b] (K)	Equilibrium	Phases in equilibrium[c]
0.220	881	0.215	891	Eutectic	L + NaF + Na_3UF_7
0.250	769	0.250	770	Lower decomposition limit	Na_3UF_7 + NaF + Na_2UF_6
0.250	801	0.250	801	α–β transition	α-Na_3UF_7 + β-Na_3UF_7
0.250	904	0.250	902	Congruent melting	L + Na_3UF_7
0.274	892	0.280	896	Eutectic	L + Na_3UF_7 + Na_2UF_6
0.327	921	0.325	921	Peritectic	L + Na_2UF_6 + $Na_5U_3F_{17}$
0.376	904	0.370	903	Lower decomposition limit	Na_2UF_6 + $Na_7U_6F_{31}$ + $Na_5U_3F_{17}$
0.363	946	0.370	946	Peritectic	L + $Na_5U_3F_{17}$ + $Na_7U_6F_{31}$
0.462	989	0.462	991	Congruent melting	L + $Na_7U_6F_{31}$
0.667	933	0.667	933	Upper decomposition limit	$Na_7U_6F_{31}$ + UF_4 + NaU_2F_9
0.565	954	0.560	953	Eutectic	L + $Na_7U_6F_{31}$ + UF_4

[a] Obtained in this study.
[b] Experimentally determined by Barton et al. [20].
[c] Symbol 'L' refers to liquid.

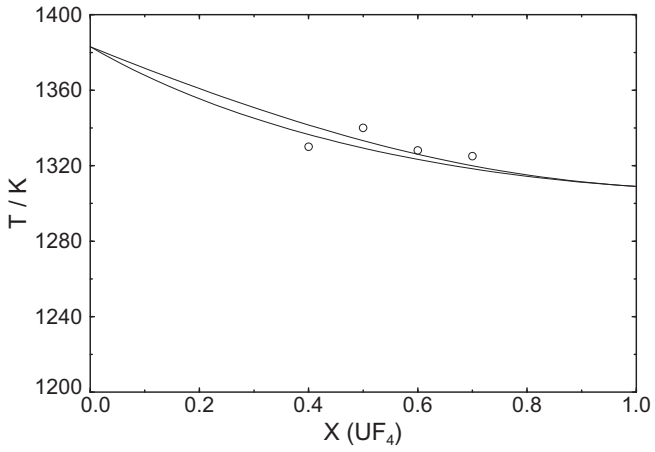

Fig. 5. The optimized ThF_4–UF_4 phase diagram; ○ thermal analysis data obtained by Weaver et al. [21].

one assessed by van der Meer et al. [22] using a general polynomial formalism for the description of the excess Gibbs parameters of solid and liquid solutions.

4. Ternary systems

4.1. The LiF–NaF–ThF_4 system

The calculated LiF–NaF–ThF_4 system is shown in Fig. 6. It consists of ten invariant equilibria and one saddle point, all of them summarized in Table 7. The obtained phase diagram agrees well with the one suggested by Thoma [23] which was based on the experimental results obtained using the thermal analysis and thermal gradient quenching experiments. The lowest melting temperature calculated in this study was found at 782 K which is only 4 K higher than the lowest eutectic found by Thoma. Fig. 7 shows an isothermal plot of the LiF–NaF–ThF_4 phase diagram calculated at 873 K showing a good correlation to the one published by Thoma.

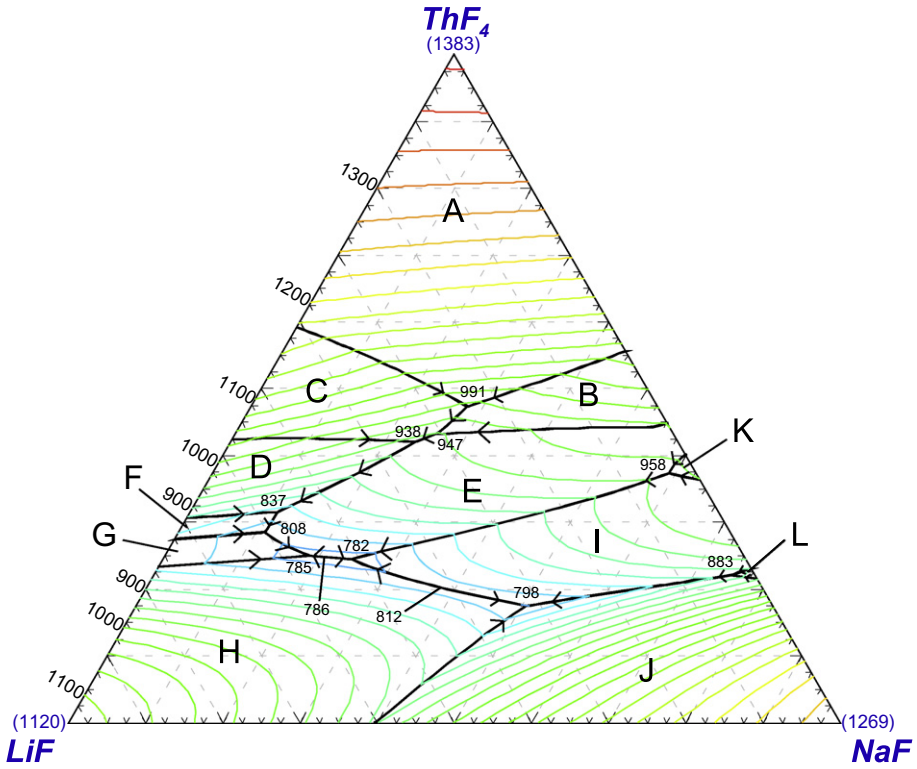

Fig. 6. Calculated liquidus projection of the LiF–NaF–ThF_4 system. Isothermals and the invariant equilibria are labeled in K with the interval of 25 K. Primary phase fields: (A) ThF_4; (B) $NaTh_2F_9$; (C) $LiTh_4F_{17}$; (D) $LiTh_2F_9$; (E) $(Li,Na)_7Th_6F_{31}$ (s.s.); (F) $Li_7Th_6F_{31}$; (G) Li_3ThF_7; (H) (Li,Na)F (s.s.); (I) Na_2ThF_6; (J) (Li,Na)F (s.s.).

Table 7
Calculated invariant and singular equilibria of the LiF–NaF–ThF_4 system. Temperature is reported in K.

x_{LiF}	x_{NaF}	x_{ThF_4}	T_{calc}	Equilibrium	Solid phases present
0.246	0.280	0.474	991	Quasi-peritectic	ThF_4 + $LiTh_4F_{17}$ + $NaTh_2F_9$
0.308	0.260	0.432	947	Quasi-peritectic	(Li, Na)$_7Th_6F_{31}$ (s.s.) + $LiTh_4F_{17}$ + $NaTh_2F_9$
0.339	0.240	0.421	938	Quasi-peritectic	(Li, Na)$_7Th_6F_{31}$ (s.s.) + $LiTh_4F_{17}$ + $LiTh_2F_9$
0.034	0.592	0.374	958	Quasi-peritectic	(Li, Na)$_7Th_6F_{31}$ (s.s.) + Na_2ThF_6 + $Na_3Th_2F_{11}$
0.571	0.113	0.316	837	Quasi-peritectic	(Li, Na)$_7Th_6F_{31}$ (s.s.) + $LiTh_2F_9$+$Li_7Th_6F_{31}$
0.603	0.112	0.285	808	Quasi-peritectic	(Li, Na)$_7Th_6F_{31}$ (s.s.) + Li_3ThF_7 + $Li_7Th_6F_{31}$
0.562	0.188	0.250	785	Eutectic	(Li, Na)$_7Th_6F_{31}$ (s.s.) + Li_3ThF_7 + (Li, Na)F (s.s.)
0.511	0.243	0.246	782	Eutectic	(Li, Na)$_7Th_6F_{31}$ (s.s.) + Na_2ThF_6 + (Li, Na)F (s.s.)
0.321	0.504	0.175	798	Eutectic	Na_2ThF_6 + (Li, Na)F (s.s.1) + (Li, Na)F (s.s.2)
0.031	0.749	0.220	883	Quasi-peritectic	Na_2ThF_6 + (Li, Na)F (s.s.) + Na_4ThF_8
0.551	0.200	0.249	786	Saddle point	
0.404	0.397	0.199	812	Saddle point	

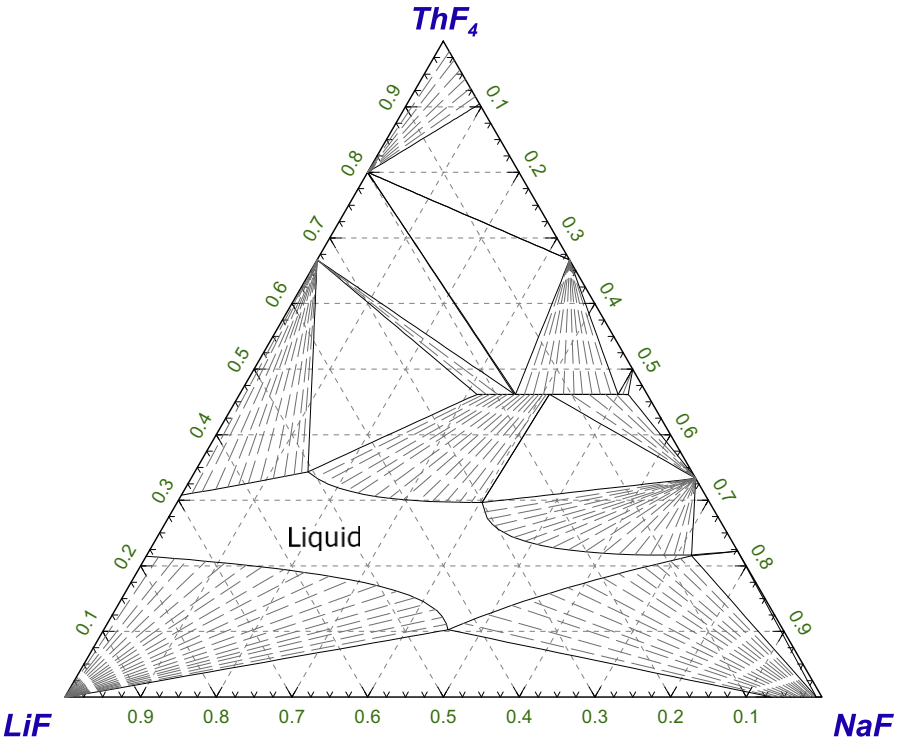

Fig. 7. The isothermal plot of the LiF–NaF–ThF_4 phase diagram calculated at 873 K.

No ternary stoichiometric compounds have been observed experimentally in the LiF–NaF–ThF_4 system, however, a pseudo-binary (Li, Na)$_7Th_6F_{31}$ solid solution at the sodium rich side has been reported by Thoma suggesting a maximum solubility limit at 1:1 composition, in agreement with our calculation. No solubility of Na in $Li_7Th_6F_{31}$ has been observed.

4.2. The LiF–NaF–UF_4 system

Fig. 8 shows the optimized LiF–NaF–UF_4 phase diagram obtained in this study. It consists of ten invariant equilibria; two eutectics, seven quasi-peritectics and one peritectic. One saddle point between the Na_2UF_6 and (Li, Na)F solid solution primary crystallization fields has been found. The temperatures and the exact compositions of all calculated equilibria are reported in Table 8. The phase diagram obtained in this study is in good correlation to the one suggested by Thoma et al. [14] who used thermal analysis and quenching experiments for their phase equilibrium studies. The only slight disagreement appears in the middle part of the phase diagram where Thoma et al. found a narrow field of primary crystallization of the NaU_2F_9 compound whereas in our calculation this field was not reproduced. However, due to the very small range of this field it hardly affects the shape of the liquidus surface. The lowest melting temperature found in our work is at 718 K and X(LiF) = 0.570, X(NaF) = 0.164, $X(UF_4)$ = 0.284, in a good agreement to the experimental value which corresponds to the same temperature and X(LiF) = 0.435, X(NaF) = 0.243, $X(UF_4)$ = 0.322. Similarly as in case of the previously discussed LiF–NaF–ThF_4 system there are no intermediate compounds reported. The only ternary solid phase appearing in this system is the (Li, Na)$_7U_6F_{31}$ solid solution which was found to have limited solubilities at both $Li_7U_6F_{31}$ and $Na_7U_6F_{31}$ rich corners.

4.3. The LiF–ThF_4–UF_4 system

The LiF–ThF_4–UF_4 phase diagram has been investigated in detail by Weaver et al. [21] and has been thermodynamically assessed by van der Meer et al. [22] using a polynomial formalism for the description of both liquid and solid solutions. It contains three invariant equilibria, two eutectics and one quasi-peritectic. No ternary stochiometric compounds have been found in this system, but as reported by Weaver et al. four solid solutions appear in the ternary field and these significantly influence the shape of the liquidus surface of the LiF–ThF_4–UF_4 phase diagram. Therefore,

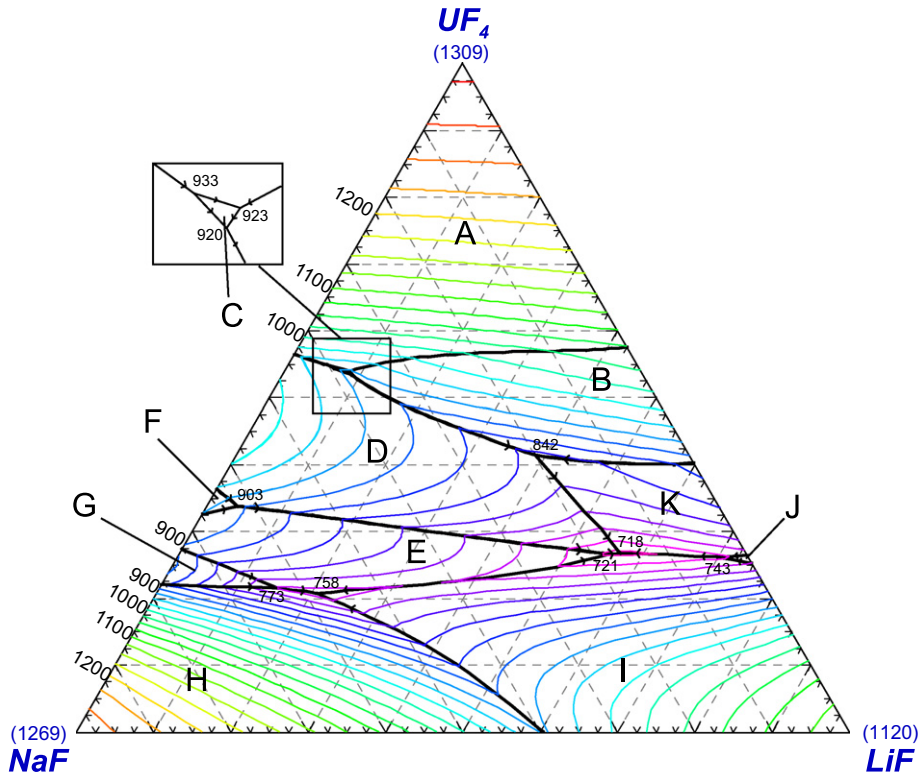

Fig. 8. Calculated liquidus projection of the LiF–NaF–UF_4 system. Isothermals and the invariant equilibria are labeled in K with the interval of 25 K. Primary phase fields: (A) UF_4; (B) LiU_4F_{17}; (C) NaU_2F_9; (D) $(Li, Na)_7U_6F_{31}$ (s.s.); (E) Na_2UF_6; (F) $Na_5U_3F_{17}$; (G) Na_3UF_7; (H) (Li, Na)F(s.s.); (I) (Li, Na)F (s.s.); (J) Li_4UF_8; (K) $(Li, Na)_7U_6F_{31}$ (s.s.).

Table 8
Calculated invariant and singular equilibria of the LiF–NaF–UF_4 system. Temperature is reported in K.

x_{LiF}	x_{NaF}	x_{UF_4}	T_{calc}	Equilibrium	Solid phases present
0.033	0.413	0.554	933	Peritectic	UF_4 + NaU_2F_9 + $(Li, Na)_7U_6F_{31}$ (s.s.)
0.085	0.376	0.539	923	Quasi-peritectic	UF_4 + LiU_4F_{17} + NaU_2F_9
0.087	0.377	0.536	920	Quasi-peritectic	$(Li, Na)_7U_6F_{31}$ (s.s.) + LiU_4F_{17} + NaU_2F_9
0.388	0.198	0.414	842	Quasi-peritectic	LiU_4F_{17} + $(Li, Na)_7U_6F_{31}$ (s.s.1) + $(Li, Na)_7U_6F_{31}$ (s.s.2)
0.570	0.162	0.268	718	Eutectic	(Li, Na)F (s.s.) + $(Li, Na)_7U_6F_{31}$ (s.s.1) + $(Li, Na)_7U_6F_{31}$ (s.s.2)
0.555	0.179	0.266	721	Quasi-peritectic	(Li, Na)F (s.s.) + $(Li, Na)_7U_6F_{31}$ (s.s.) + Na_2UF_6
0.206	0.586	0.208	758	Eutectic	Na_2UF_6 + (Li, Na)F (s.s.1) + (Li, Na)F (s.s.2)
0.151	0.633	0.216	773	Quasi-peritectic	Na_2UF_6 + Na_3UF_7 + $(Li, Na)_7U_6F_{31}$ (s.s.)
0.041	0.621	0.338	903	Quasi-peritectic	Na_2UF_6 + (Li, Na)F (s.s.) + $Na_5U_3F_{17}$
0.698	0.040	0.262	743	Quasi-peritectic	Li_4UF_8 + (Li, Na)F (s.s.) + $(Li, Na)_7U_6F_{31}$ (s.s.)
0.328	0.452	0.219	777	Saddle point	

careful description of the excess Gibbs parameters of these four phases is necessary. The calculated LiF–ThF_4–UF_4 phase diagram obtained in this study is shown in Fig. 9 with the lowest eutectic at T = 756 K and X(LiF) = 0.738, X(ThF_4) = 0.022, X(UF_4) = 0.240, in a very good agreement to experimentally determined eutectic by Weaver et al. who found T = 761 K. The other eutectic calculated in this study was found at T = 873 K and X(LiF) = 0.627, X(ThF_4) = 0.185, X(UF_4) = 0.188 compared to T = 882 K determined by Weaver et al. whereas the quasi-peritectic was found at T = 770 K and X(LiF) = 0.740, X(ThF_4) = 0.065, X(UF_4) = 0.195 compared to T = 773 K determined by Weaver et al. Hence these two calculated equilibria are also in a good agreement with the experiment.

4.4. The NaF–ThF_4–UF_4 system

The calculated NaF–ThF_4–UF_4 phase diagram obtained in this study is shown in Fig. 10. It consists of five pseudo-ternary solid solutions that significantly determine the shape of the liquidus surface. The optimization of the excess Gibbs parameters of these solutions was based on the experimentally determined invariant equilibria published by Thoma et al. [15] as well as on the overall shape of the phase diagram as shown in the same study. In total seven invariant equilibria were found in the optimized NaF–ThF_4–UF_4 phase diagram which are summarized in Table 9 giving their exact compositions, temperatures and the solid phases in equilibrium. The lowest eutectic was found at T = 851 K which is in good agreement to the lowest melting temperature (T = 858 K) found in the work by Thoma et al. [15].

5. Nuclear fuel optimization

The main aim of this study is the investigation of the nuclear fuel properties of the Molten Salt Fast Reactor (MSFR) concept [1] which can be deduced once the thermodynamic database is available. In the above mentioned sections the full thermodynamic description of the LiF–NaF–ThF_4–UF_4 system has been made and in this section these data will be used to optimize and discuss the

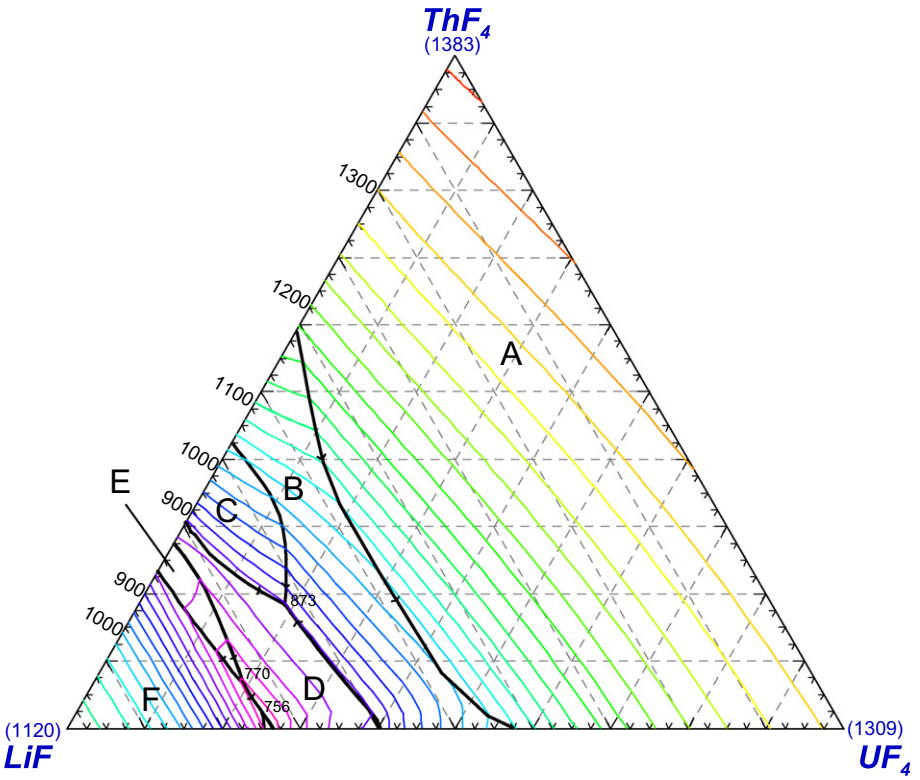

Fig. 9. Calculated liquidus projection of the $LiF–ThF_4–UF_4$ system. Isothermals and the invariant equilibria are labeled in K with the interval of 25 K. Primary phase fields: (A) (Th, U)F_4(s.s.); (B) Li(Th, U)$_4F_{17}$ (s.s.); (C) Li(Th, U)$_2F_9$ (s.s.); (D) Li_7(Th, U)$_6F_{31}$ (s.s.); (E) Li_3(Th, U)F_7; (F) LiF.

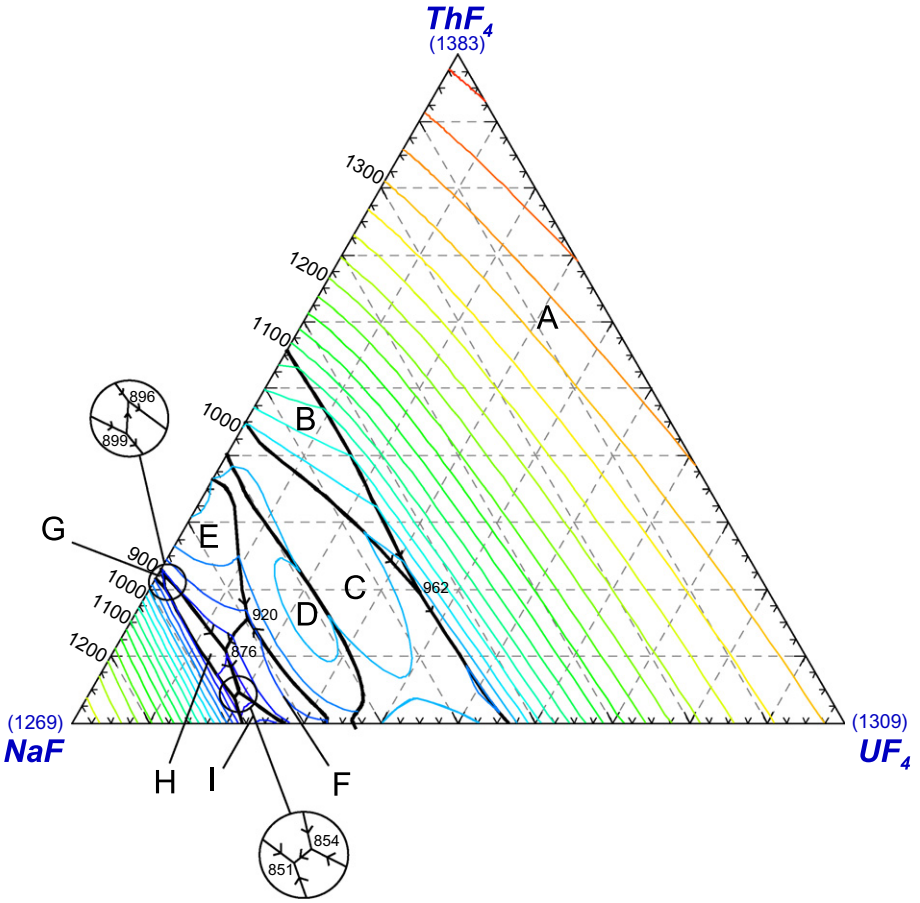

Fig. 10. Calculated liquidus projection of the $NaF–ThF_4–UF_4$ system. Isothermals and the invariant equilibria are labeled in K with the interval of 25 K. Primary phase fields: (A) (Th, U)F_4 (s.s.); (B) Na(Th, U)$_2F_9$ (s.s.); (C) Na_7(Th, U)$_6F_{31}$ (s.s.); (D) $Na_3Th_2F_{11}–Na_5U_3F_{17}$ (s.s.); (E) Na_2(Th, U)F_6 (s.s.1); (F) Na_2(Th, U)F_6 (s.s.2); (G) Na_4ThF_8; (H) Na_7(Th, U)$_2F_{15}$ (s.s.); (I) Na_3UF_7.

Table 9
Calculated invariant and singular equilibria of the NaF–ThF_4–UF_4 system. Temperature is reported in K.

x_{NaF}	x_{ThF_4}	x_{UF_4}	T_{calc}	Equilibrium	Solid phases present
0.453	0.195	0.353	962	Quasi-peritectic	(Th, U)F_4 (s.s.) + Na(Th, U)$_2F_9$ (s.s.) + Na_7(Th, U)$_6F_{31}$ (s.s.)
0.695	0.156	0.149	920	Quasi-peritectic	Na_2(Th, U)F_6 (s.s.1) + Na_2(Th, U)F_6 (s.s.2) + $Na_3Th_2F_{11}$–$Na_5Th_3F_{17}$ (s.s.)
0.748	0.108	0.144	876	Quasi-peritectic	Na_2(Th, U)F_6 (s.s.1) + Na_2(Th, U)F_6 (s.s.2) + Na_7(Th, U)$_2F_{15}$ (s.s.)
0.770	0.222	0.008	896	Quasi-peritectic	Na_2(Th, U)F_6 (s.s.) + Na_4ThF_8 + Na_7(Th, U)$_2F_{15}$ (s.s.)
0.779	0.203	0.018	899	Peritectic	NaF + Na_4ThF_8 + Na_7(Th, U)$_2F_{15}$ (s.s.)
0.761	0.046	0.193	854	Quasi-peritectic	Na_2(Th, U)F_6 (s.s.) + Na_3UF_7 + Na_7(Th, U)$_2F_{15}$ (s.s.)
0.771	0.038	0.191	851	Eutectic	NaF + Na_3UF_7 + Na_7(Th, U)$_2F_{15}$ (s.s.)

MSFR fuel choice. Moreover it will be also shown how addition of another component into the fuel solvent, in this case NaF, can affect the melting behaviour of the fuel.

One of the main criteria when defining a fuel for a molten salt reactor is its melting temperature. In order to keep sufficient safety margin it is generally accepted within a molten salt community that the melting temperature of the fuel should be at least 50 K lower than the designed inlet temperature of a reactor. One could also simplify that the lower the melting temperature the better it is for the two following reasons. First, it decreases the risk of a system freezing under certain circumstances and second, having a bigger temperature difference between the exit and inlet temperature of a reactor results in a higher thermal efficiency of the power plant. Of course this could be done by increasing the outlet temperature, but this one is limited by the corrosion rate of the structural materials which increases with temperature. New alloys that would withstand higher temperatures are nowadays under investigations, but for a time being the upper temperature limit of a molten salt reactor is around 1073 K. In the MSFR concept the designed operating temperatures of the reactor are rather high, 973 K on inlet and 1123 K on exit [24]. This is due to the fact that a single-component solvent (^{7}LiF) has been selected for the dissolution of actinides. The MSFR concept is a breeder reactor which is based on the ^{232}Th/^{233}U cycle. Both actinides are dissolved in a form of tetra-fluorides and when optimizing the fuel choice using the thermodynamic database the concentrations of these actinide components must be close to the value determined by the reactor designers in order to keep the breeding ratio above 1. This concentration criterion has been taken into account during the optimization of the fuel choice as discussed further.

The initial fuel salt of the MSFR concept contains fertile $^{232}ThF_4$ and fissile $^{233}UF_4$ of total concentration 22.5 mol% which was set based on the eutectic point in the binary LiF–ThF_4 system. According to the neutronic calculations performed by Merle-Lucotte et al. [24] the concentration of fissile $^{233}UF_4$ ranges from 2.4 mol% to 2.7 mol%. Taking the average value (2.55 mol% of $^{233}UF_4$) the overall composition of the initial fuel salt is LiF–ThF_4–UF_4 (77.50–19.95–2.55 mol%).

This composition is represented by a dashed line in Fig. 11 which shows the calculated LiF–ThF_4 pseudo-binary phase diagram with fixed amount of UF_4 set to 2.55 mol%. The liquidus temperature of such composition is T = 854 K as demonstrated by 'A' point in the figure. One can also see that only a slight shift (~1 mol%) of the initial composition towards the ThF_4 side results in the lowest melting temperature (T = 835 K) of this pseudo-binary system. This point ('B' in the figure) corresponds to the LiF–ThF_4–UF_4 (76.4–21.05–2.55) composition. Since as low melting temperature of the fuel as possible is desired for the molten salt reactor and because the concentration of the actinide tetra-fluorides is close to the initially calculated one for the MSFR concept this point would be our recommended fuel composition for the MSFR when based only on the LiF–ThF_4–UF_4 system. Keeping the above mentioned 50 K safety margin the inlet temperature of a reactor using this salt composition can be 885 K.

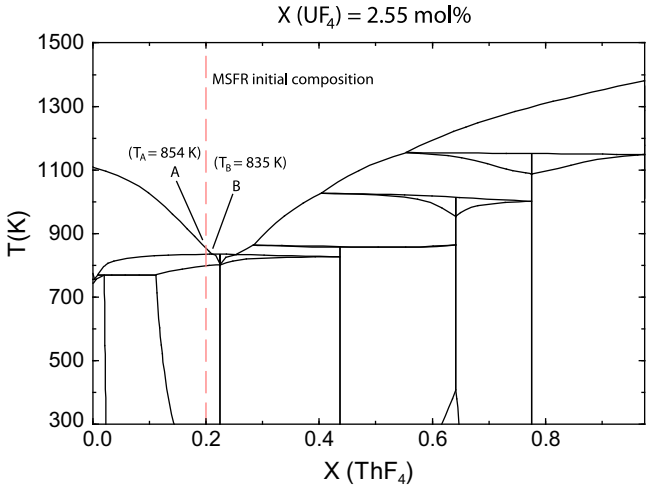

Fig. 11. The calculated LiF–ThF_4 pseudo-binary phase diagram with fixed concentration of UF_4 set to 2.55 mol%.

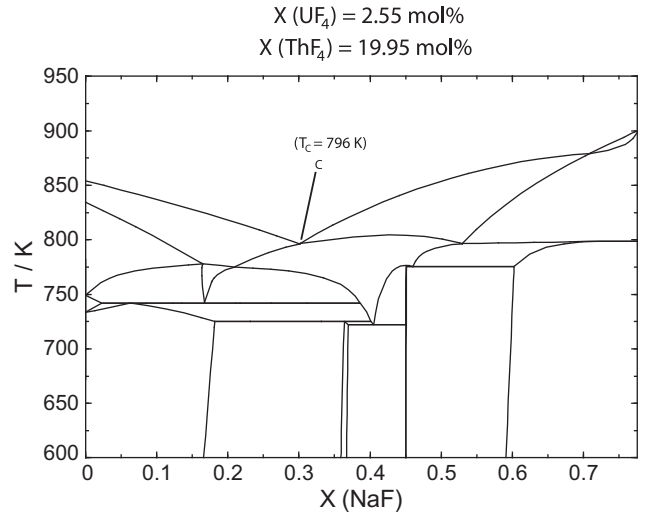

Fig. 12. The calculated LiF–NaF pseudo-binary phase diagram with fixed concentration of ThF_4 and UF_4 set to 19.95 mol% and 2.55 mol% respectively.

In the next step we calculated the influence on the melting behaviour of the fuel when adding another component to the fuel solvent. Due to different neutron capture cross sections of various cations the selection of possible components for the fuel is somewhat limited. In case of thermal breeder reactors (e.g. Molten Salt Breeder Reactor [25]) where the neutron economy is very strict the selection is limited to only ^{7}Li and Be with very low cross sections $\sigma_{thermal}$ = 0.045 barn and $\sigma_{thermal}$ = 0.0088 barn respectively. However, since the MSFR concept is non-moderated reactor design the neutron spectrum is kept in the epi-thermal range with a less

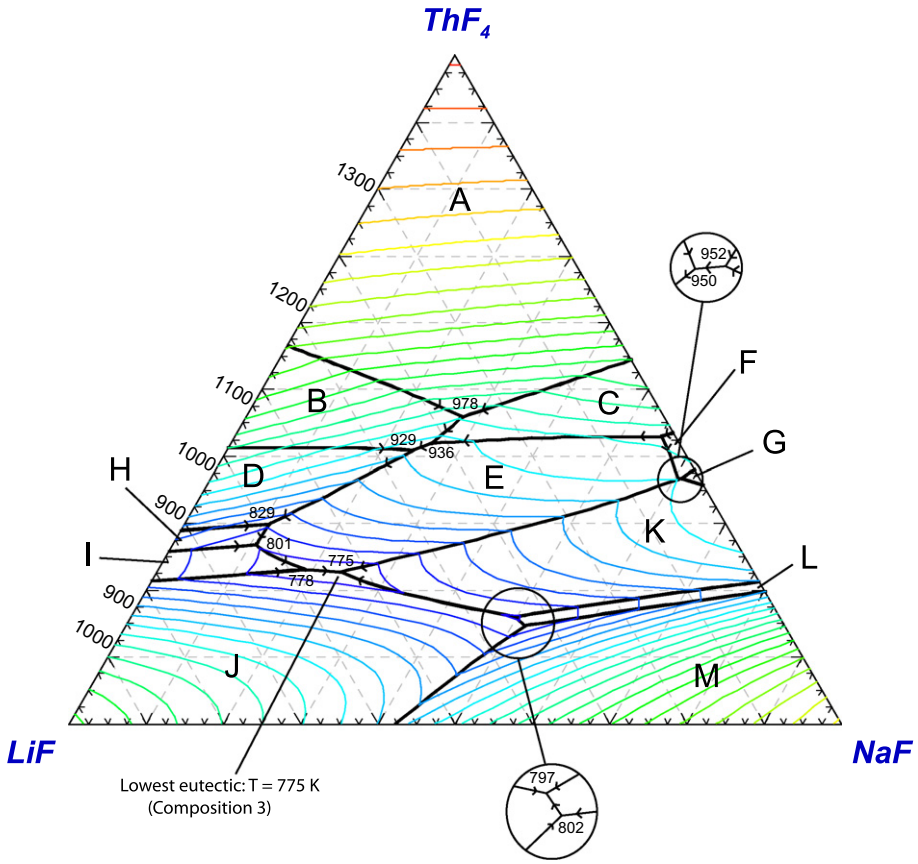

Fig. 13. The calculated LiF–NaF–ThF_4 pseudo-ternary phase diagram with fixed concentration of UF_4 set to 2.55 mol%. Primary phase fields: (A) (U, Th)F_4 (s.s.); (B) Li(Th, U)$_4F_{17}$ (s.s.); (C) Na(Th, U)$_2F_9$ (s.s.); (D) Li(Th, U)$_2F_9$ (s.s.); (E) (Li, Na)$_7$Th$_6F_{31}$ (s.s.); (F) Na$_7$(Th, U)$_6F_{31}$ (s.s.); (G) $Na_3Th_2F_{11}$–$Na_5U_3F_{17}$ (s.s.); (H) Li$_7$(Th, U)$_6F_{31}$ (s.s.); (I) Li$_3$(Th, U)F_7 (s.s.); (J) (Li, Na)F (s.s.); (K) Na$_2$(Th, U)F_6 (s.s.); (L) Na$_7$(Th, U)$_2F_{15}$ (s.s.); (M) (Li, Na)F (s.s.).

sensitive neutron economy and other cations, among them Na, can be used as part of the fuel matrix. Therefore, we could consider NaF as a possible candidate to decrease the melting temperature of the MSFR fuel.

As mentioned above, one should avoid large departures from the initial actinide concentrations when optimizing the fuel choice. Hence the 'easiest' is to calculate the LiF–NaF pseudo-binary system with fixed concentrations of ThF_4 and UF_4 at 19.95 mol% and 2.55 mol% respectively. Such phase diagram is shown in Fig. 12 showing the lowest melting temperature at T = 796 K (point 'C' in the figure) corresponding to the LiF–NaF–ThF_4–UF_4 (47.40–30.10–19.95–2.55) composition. Thus addition of 30 mol% to the initial MSFR fuel salt decreases the melting temperature by nearly 60 K. We consider this composition a potential fuel for MSFR.

In the last step, we have allowed variation of the ThF_4 concentration while keeping the UF_4 amount fixed to initial 2.55 mol%. Fig. 13 shows the calculated liquidus projection of the LiF–NaF–ThF_4 system with constant concentration of UF_4 at 2.55 mol%. It consists of twelve invariant equilibria with the lowest pseudo-ternary eutectic found at LiF–NaF–ThF_4–UF_4 (52.15–23.18–22.12–2.55) composition and T = 775 K. This point contains 'only' around 2 mol% more of ThF_4 which can be acceptable amount in order to lower the melting temperature of the MSFR fuel by almost 80 K. We consider this composition as third recommended fuel selection based on the thermodynamic assessment performed in this study.

6. Nuclear fuel properties

In the previous section, the optimization of the nuclear fuel for the MSFR concept has been done according to the developed thermodynamic database and three possible fuel compositions have been proposed. These are:

(1) the NaF free LiF–ThF_4–UF_4 (76.4–21.05–2.55) composition and
(2) the LiF–NaF–ThF_4–UF_4 (47.40–30.10–19.95–2.55) composition and
(3) the LiF–NaF–ThF_4–UF_4 (52.15–23.18–22.12–2.55) composition.

The melting behaviour of both salts has been already discussed in Section 5 giving the melting temperature of Composition 1 at T = 835 K, T = 796 K for Composition 2 and T = 775 K for Composition 3. Especially the latter two temperatures are significantly lower than the melting temperature of the initial fuel choice found at T = 854 K.

Furthermore using the thermodynamic data obtained in this study together with the data for the gaseous species presented in Table 4 the vapour pressures of all three recommended fuel compositions plus the initial MSFR composition have been determined as a function of temperature and the corresponding equations are given in Table 10. The observed vapour pressures are very similar for all compositions following nearly the same slope as shown in Fig. 14. Moreover they possess low values (in order of Pascals) in the operating temperatures of a molten salt reactor and that is essential as no composition shift due to the incongruent vaporization can occur in the fuel salt. This is very important for a molten salt reactor as possible composition shift could result in a solid precipitation which could cause local hot spots. The calculated boiling temperatures of all considered compositions have

Table 10
Calculated fuel properties of the recommended fuel compositions as well as the initial composition of the MSFR.

Properties	Initial MSFR	Composition 1	Composition 2	Composition 3
Composition	LiF–ThF_4–UF_4 (77.50–19.95–2.55)	LiF–ThF_4–UF_4 (76.4–21.05–2.55)	LiF–NaF–ThF_4–UF_4 (47.40–30.10–19.95–2.55)	LiF–NaF–ThF_4–UF_4 (52.15–23.18–22.12–2.55)
Melting temperature (K)	854	835	796	775
Vapour pressure $\log_{10}$ (p/Pa)	11.569–12,774/(*T*/*K*)	11.500–12,732/(*T*/*K*)	11.274–12,577/(*T*/*K*)	11.274–12,606/(*T*/*K*)
Boiling temperature (K)	2021	2018	2056	2041

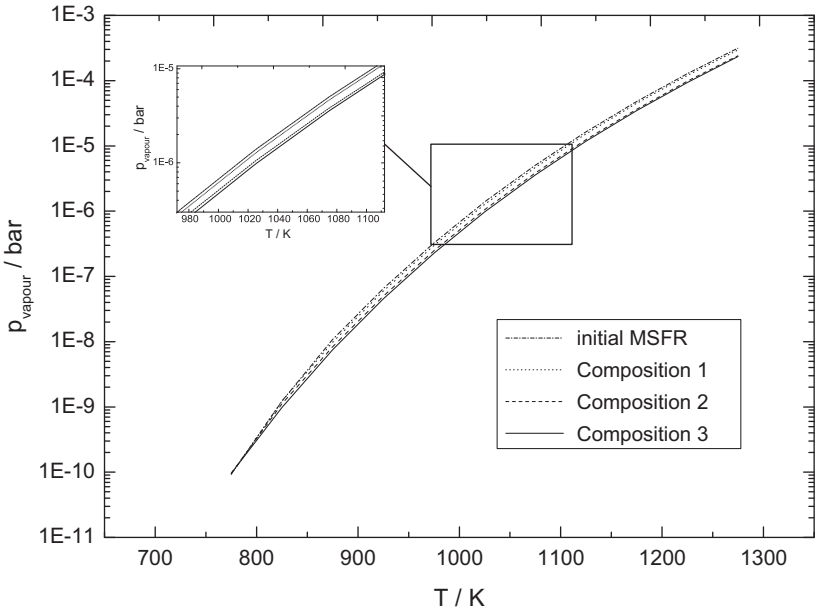

Fig. 14. The calculated vapour pressure of the initial MSFR fuel composition in comparison with our recommended fuel choices. The inset graph shows in better details the small difference between the various compositions.

been found above 2000 K, their exact values are reported in Table 10.

7. Summary

In this study, the full thermodynamic description of the LiF–NaF–ThF_4–UF_4 system has been made and as discussed in Sections 3 and 4 a very good correlation between our assessment and the experimental data from literature has been achieved. Based on obtained results the fuel of the molten salt fast reactor concept has been optimized and three different compositions have been suggested. Furthermore the melting behaviour, the vapour pressure and the boiling temperature of all these compositions have been determined showing very promising values according to molten salt reactor criteria. The obtained results are summarized in Table 10 in comparison to the properties of the initial MSFR composition calculated in this study as well. One of the highlights of this work is the observation that using the binary LiF–NaF solvent for the dissolution of AnF_4 (An = Th, U) instead of only pure LiF solvent lowers the melting temperature by 60 K as seen from the comparison of the properties between Composition 1 fuel and Composition 3 fuel.

Acknowledgement

M.B. acknowledges the European Commission for support given in the frame of the program "Training and Mobility of Researchers".

References

[1] S. Delpech, E. Merle-Lucotte, D. Heuer, M. Allibert, V. Ghetta, C. Le-Brun, X. Doligez, G. Picard, J. Fluor. Chem. 130 (2009) 11–17.
[2] O. Beneš, R.J.M. Konings, J. Nucl. Mater. 375 (2008) 202–208.
[3] O. Beneš, R.J.M. Konings, J. Nucl. Mater. 377 (3) (2008) 449–457.
[4] O. Beneš, R.J.M. Konings, J. Chem. Thermodyn. 41 (2009) 1086–1095.
[5] C.W. Bale, et al., FactSage Software v. 5.5.
[6] M.W. Chase Jr., (Ed.), NIST-JANAF Thermochemical Tables, Part I, Al-Co, fourth ed., vol. 9, J. Phys. Chem. Ref. Data Monograph, 1998.
[7] R.J.M. Konings, J.P.M. van der Meer, E. Walle, Chemical Aspects of Molten Salt Reactor Fuel, Tech. Rep., ITU-TN 2005/25, 2005.
[8] O. Beneš, R.J.M. Konings, Comput Coup Phase Diag Thermochem 32 (2008) 121–128.
[9] A.D. Pelton, P. Chartrand, G. Eriksson, Metall. Trans. A 32 (2001) 1409–1416.
[10] P. Chartrand, A.D. Pelton, Metall. Trans. A 32 (2001) 1397–1407.
[11] P. Chartrand, A.D. Pelton, Metall. Trans. A 32 (2001) 1385.
[12] O. Beneš, J.P.M. van der Meer, R.J.M. Konings, Comput Coup Phase Diag Thermochem 31 (2007) 209–216.
[13] R.J.M. Konings, L.R. Morss, J. Fuger, The Chemistry of the Actinide and Transactinide Elements, vol. 4, Springer, Dordrecht, The Netherlands, 2006 (Chapter 19).
[14] R.E. Thoma, H. Insley, B.S. Landau, H.A. Friedman, W.R. Grimes, J. Am. Ceram. Soc. 42 (1959) 21.
[15] R.E. Thoma, H. Insley, G.M. Hebert, H.A. Friedman, C.F. Weaver, J. Am. Ceram. Soc. 46 (1963) 37–42.
[16] R.E. Thoma, H. Insley, B.S. Landau, H.A. Friedman, W.R. Grimes, J. Phys. Chem. 63 (1959) 1266.
[17] R.E. Thoma, Advances in Molten Salt Chemistry, vol. 3, Plenum Press, 1975 (Chapter 6).
[18] L.A. Harris, G.D. White, R.E. Thoma, J. Phys. Chem. 63 (1959) 1974–1975.
[19] J. van der Meer, R.J.M. Konings, M.H.G. Jacobs, H.A.J. Oonk, J. Nucl. Mater. 344 (2005) 94–99.
[20] C.J. Barton, H.A. Friedman, W.R. Grimes, H. Insley, R.E. Moore, R. Thoma, J. Am. Ceram. Soc. 41 (1958) 66.

[21] C.F. Weaver, R.E. Thoma, H. Insley, H.A. Friedman, J. Am. Ceram. Soc. 43 (1960) 213.
[22] J. van der Meer, R.J.M. Konings, H.A.J. Oonk, J. Nucl. Mater. 357 (2006) 48–57.
[23] R.E. Thoma, J. Inorg. Nucl. Chem. 34 (1972) 2747–2760.
[24] E. Merle-Lucotte, D. Heuer, M. Allibert, X. Doligez, V. Ghetta, Minimizing the fissile inventory of the molten salt fast reactor, in: Advances in Nuclear Fuel Management IV (ANFM 2009), LaGrange Park, IL, USA, 2009.
[25] R.C. Robertson, Technical Report ORNL-4541, Tech. Rep., 1971.